energies

MDPI

Article

Experimental Study on Utilizing Silica Gel with Ethanol and Water for Adsorption Heat Storage

Ahmed Rezk [1], Abdul Ghani Olabi [2,*], Abdul Hai Alami [2], Ali Radwan [2,3], Hasan Demir [4], Shek Mohammod Atiqure Rahman [2], Sheikh Khaleduzzaman Shah [5,*] and Mohammad Ali Abdelkareem [2,6,*]

1 Energy and Bioproducts Research Institute (EBRI), College of Engineering and Physical Science, Aston University, Birmingham B4 7ET, UK
2 Sustainable Energy & Power Systems Research Centre, RISE, University of Sharjah, Sharjah P.O. Box 27272, United Arab Emirates
3 Mechanical Power Engineering Department, Mansoura University, Mansoura 35516, Egypt
4 Department of Chemical Engineering, Osmaniye Korkut Ata University, 80000 Osmaniye, Turkey
5 Renewable Energy and Energy Efficiency Group, Department of Infrastructure Engineering, Faculty of Engineering and Information Technology, The University of Melbourne, Melbourne, VIC 3010, Australia
6 Chemical Engineering Department, Minia University, Minya 61519, Egypt
* Correspondence: aolabi@sharjah.ac.ae (A.G.O.); sheikhkhaleduzzaman.shah@unimelb.edu.au (S.K.S.); mabdulkareem@sharjah.ac.ae (M.A.A.)

Abstract: Adsorption heat storage is the most feasible technology for heating decarbonization, which can store large quantities of waste and renewable heat for an exceptionally long time. However, utilizing adsorption heat storage in geographical locations with sub-zero ambient conditions is challenging. Therefore, this paper experimentally investigates the use of ethanol as a working fluid paired with silica gel for adsorption heat storage and utilizes sub-zero ambient as the heat source. The heat storage characteristics, heat charging/discharging cyclic performance, and energy conversion performance via exergy analysis were determined under realistic operating conditions and benchmarked against the widely investigated silica gel/water. Ethanol adsorbate was successfully utilized as a working fluid to employ the evaporators operating under sub-zero ambient conditions. Silica gel/ethanol showed the most significant net cyclic uptake, twice that of silica gel/water. However, the physical characteristics of ethanol molecules led to a degree of non-desorbed fluid, which hampered such potential to store 18.08 kJ/kg_{ads} under a sub-zero evaporator temperature and 24.84 kJ/kg_{ads} for an above-zero evaporator temperature compared to silica gel of 155.12 kJ/kg_{ads} operating an above-zero evaporator temperature. On the other hand, silica gel/ethanol showed the fastest heat charging/discharging rate that can shorten the cycle time by 45%. The major contributor to exergy destruction was the exergy transferred by charging heat, which was five times the discharging heat due to the high charging temperature.

Keywords: heat storage; adsorption; silica gel; ethanol; water; heat storage capacity

check for updates

Citation: Rezk, A.; Olabi, A.G.; Alami, A.H.; Radwan, A.; Demir, H.; Rahman, S.M.A.; Shah, S.K.; Abdelkareem, M.A. Experimental Study on Utilizing Silica Gel with Ethanol and Water for Adsorption Heat Storage. *Energies* **2023**, *16*, 444. https://doi.org/10.3390/en16010444

Academic Editors: Ron Zevenhoven and Jian Liu

Received: 27 October 2022
Revised: 10 November 2022
Accepted: 26 December 2022
Published: 30 December 2022

Copyright: © 2022 by the authors. Licensee MDPI, Basel, Switzerland. This article is an open access article distributed under the terms and conditions of the Creative Commons Attribution (CC BY) license (https://creativecommons.org/licenses/by/4.0/).

1. Introduction

Severe environmental impacts from the heavy usage of fossil fuels have led to profound health issues and climate change [1,2]. Therefore, many strategies have been proposed to overcome such problems, such as improving the efficiency of the current processes through waste heat recovery [3,4], applying efficient environmentally friendly devices, such as fuel cells [5], and utilizing renewable energy sources. Renewable energy sources, such as solar thermal [6,7], solar PV [8], geothermal [9,10], and wind [11] are the most promising, as they can provide sustainable and clean energy. However, the rapid growth in the capacities of the different renewable energy sources requires advances in renewable energy

storage systems that can accommodate, such growing capabilities. Therefore, thermal energy storage (TES) is the cornerstone for utilizing waste, and renewable heat sources to meet the heating decarbonization and net-zero goals [12,13]. This also aligns with the UN Sustainable Development Goal-11 "Sustainable Cities and Communities" and Goal-13 "Climate Action". TES is crucial to address the mismatch between the heat sources and demand and utilize the low-grade heat when it is unfeasible to utilize the conventional thermodynamic cycles due to the narrow temperature difference between the heat source and sink [14]. In addition to the energy conversion deficiency due to converting one form of energy (e.g., heat) to another (e.g., mechanical work for electricity production), utilizing low-grade heat adds enormous complications to the used thermodynamic cycle, meaning that it is more advantageous to reuse such renewable heat directly for other purposes [15].

TES technologies are classified primarily into sensible, latent, and thermochemical; thermochemical TES can be subcategorized into two groups: chemical reaction without sorption and sorption [16,17]. Sensible TES stores the heat by the temperature difference potential, and the heat storage density is a strong function of the storage medium's specific heat, whether it is a solid or liquid medium. Examples of sensible TES are water, liquid metals, bricks, soil, and concrete blocks. Despite its high technological readiness level, simplicity, and the wide range of materials available for sensible TES, it is inefficient due to the low heat storage density, slow heat charging/discharging processes, heat storage degradation due to the temperature difference potential, and the disrupting temperature swing at the end discharging process [18,19]. Therefore, researchers strived to enhance the heat transfer performance and the magnitude of heat stored in sensible TES by utilizing, for example, nanofluids as a heat storage medium [20,21].

Latent TES stores the heat in the heat primarily during the material's phase change, otherwise known as phase change material (PCM) TES. PCMs are categorized into (1) organic PCMs (e.g., fatty acids, paraffin wax, alkanes) and (2) inorganic (e.g., salts, ice). Although latent TES density is nearly 40% higher than the sensible TES, it suffers from low thermal diffusivity (i.e., slow charging/discharging processes), flammability of organic PCMs, and long-term instability experienced by phase segregation [22,23]. Furthermore, heat storage degradation becomes challenging if the desired latent heat temperature differs from the ambient, which is most likely in real-life applications.

Among the TES technologies, sorption TES is the most promising, primarily due to its heat storage density (nearly 70% more than sensible TES) and its ability to store the heat in the form of sorption potential; hence, it is the only suitable technology for short-to-long-term heat storage without degradation [16,24,25]. Generally, the term sorption refers to either adsorption or absorption. The former is regarded as more practical and stores the heat over a wide temperature range, making it suitable for space heating or industrial processes and the most suitable for utilizing low-grade heat sources [26]. Adsorption heat storage, therefore, utilizes adsorption pairs of porous material and working fluid, such as silica gel/water, zeolite/water, and MOF/water.

Despite the practicality of porous materials as parent adsorbents, scientists investigated metal salt encapsulation (i.e., impregnation) into porous matrixes to form composites of intensified heat storage density [27]. Examples of such composite adsorbents are encapsulating lithium bromide into silica gel and activated carbon to utilize water as a working fluid, which intensified the heat storage density by up to 381 kWh/m^3 [28]. D'Ans et al. [29] studied the encapsulation of strontium bromide ($SrBr_2$) into MIL-101(Cr), which intensified the heat storage density to 381 kWh/m^3. Moreover, Clark et al. [30] studied the strontium chloride ($SrCl_2$) encapsulated in cement, which showed a heat storage density of up to 164 kWh/m^3. It is noteworthy that cement is an uncommon host matrix for sorption application. Grekova et al. [31] studied the encapsulation of $CaCl_2$, LiCl, and LiBr into multiwall graphene nanotubes utilizing water and ethanol as working fluids, which achieved heat storage capacity of up to 445 and 470 Wh/kg for ethanol and water, respectively.

Adsorption heat storage employs an evaporator, condenser, and adsorption beds, where the evaporator utilizes the heat source via the ambient air or underground heat. De-

spite the essential need for heat storage in cold climates, far too little attention has been paid to utilizing sub-zero ambient as a heat source for the adsorption of heat storage. However, ethanol is an example of an adsorption working fluid that can operate below zero, which was previously reported for sub-zero adsorption cooling by Rezk et al. [32,33]. Therefore, the novelty of this work lies in covering such a knowledge gap by studying the heat storage potential of silica gel/ethanol to meet the heat storage demands in geographical locations of sub-zero ambient, emphasizing short-term heat storage. Accordingly, the objectives of this work are **(1)** to experimentally determine the heat storage characteristics of silica gel/ethanol; **(2)** experimentally investigate the heat charging/discharging cyclic performance of silica gel/ethanol; **(3)** undertake the exergy analysis for silica gel/ethanol to understand the energy conversion potential under realistic operating conditions; **(4)** benchmark silica gel/ethanol against the widely investigated silica gel/water pair.

2. Material and Methods

2.1. Materials

Fuji RD silica gel adsorbent was supplied by Fuji Silysia Chemical (Japan) of 2.2 mm bead diameters. The Brunauer–Emmett–Teller (BET) surface area was 820 m^2/g, and the average pore size of the silica gel was 2.2 nm. Ethanol (Ethyl alcohol C_2H_6O) 99+% and purified water adsorbates were obtained from Thermo Fisher Scientific UK.

2.2. Materials Characterization

The adsorption characteristics of the silica gel/ethanol and silica gel/water pairs were characterized using the dynamic vapor sorption (DVS) gravimetric analyzer DVS Resolution™ by Surface Measurements Systems (SMS) UK. Figure 1 shows the schematic and pictorial view of the DVS gravimetric analyzer. The apparatus measured the dynamic change of adsorbent mass every minute using a microbalance (SMS Ultrabalance™) while adsorbing the selected fluid (i.e., ethanol or water) under a controlled pressure ratio equivalent to P_{evap}/P_{ads}. A speed-of-sound sensor measured and controlled the ethanol (solvent in reservoir 2) dosage via PID mass flow controllers. An RH sensor measured and controlled the water vapor (solvent in reservoir 1) dosage via the PID mass flow controllers. The reaction and balance chambers were purged before sample loading using dry nitrogen to prevent vapor condensation. A 100 mg calibration mass was used to verify the microbalance accuracy of $\pm$0.05 mg. The key sorption characteristics of interest in this work are (1) the adsorption heat to determine the magnitude of heat storage potential and (2) the adsorption kinetics within predefined cyclic conditions to determine the realistic rate and net heat charge/discharge.

Fresh adsorbent sample (i.e., silica gel) was loaded in the reaction chamber every test and locally dried at 55 °C until reaching no change of the mass condition. The adsorbent's dry mass for the following test (i.e., reference mass) was recorded at the end of the drying process to maintain the consistency of pre-testing sample conditions. Subsequently, adsorption/desorption tests were performed at various pressure ratios, equivalent to P_{evap}/P_{ads} during heat discharging (i.e., adsorption) and P_{cond}/P_{des} during heat discharging (i.e., desorption) and temperatures to develop characteristic curves. Nitrogen was used as a carrier gas for the adsorbate vapor dosage during adsorption/desorption tests. Still, the effect of such a carrier gas on the adsorption kinetics is less than 10%, as reported by Rezk et al. [33].

Figure 2 shows the operating principle of adsorption heat storage in Figure 2a and the Clapeyron diagram in Figure 2b for the heat charging/discharging cycle. The operating conditions are usually defined by four temperatures: (1) the regeneration temperature T_{ch}, (2) the heat sink temperature T_c, (3) the heat discharge temperature T_{dis} and (4) the evaporation temperature T_e. During the charging mode, the heat at Tch regenerates the adsorbent material, and the released adsorbate vapor is condensed by releasing the heat to the heat sink at Tc. During the discharging mode, the dried adsorbent is exposed to the working fluid, and the adsorption heat at T_{dis} is used in the intended process, such as space heating, while the heat source at T_e supplies heat to the evaporator.

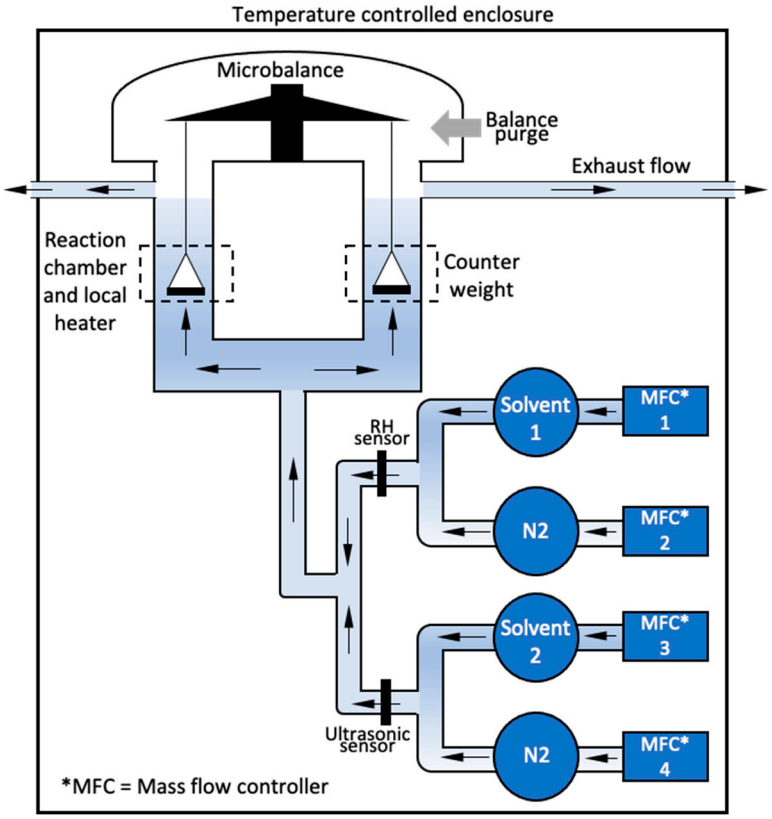

(**a**)

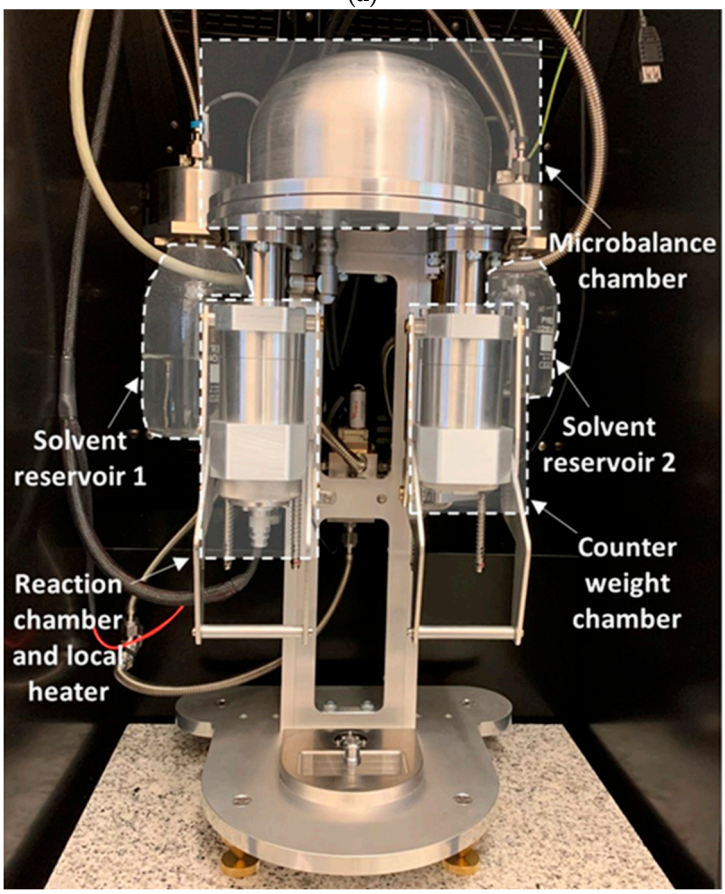

(**b**)

Figure 1. Dynamic vapor sorption analyzer (**a**) schematic diagram and (**b**) pictorial view [32].

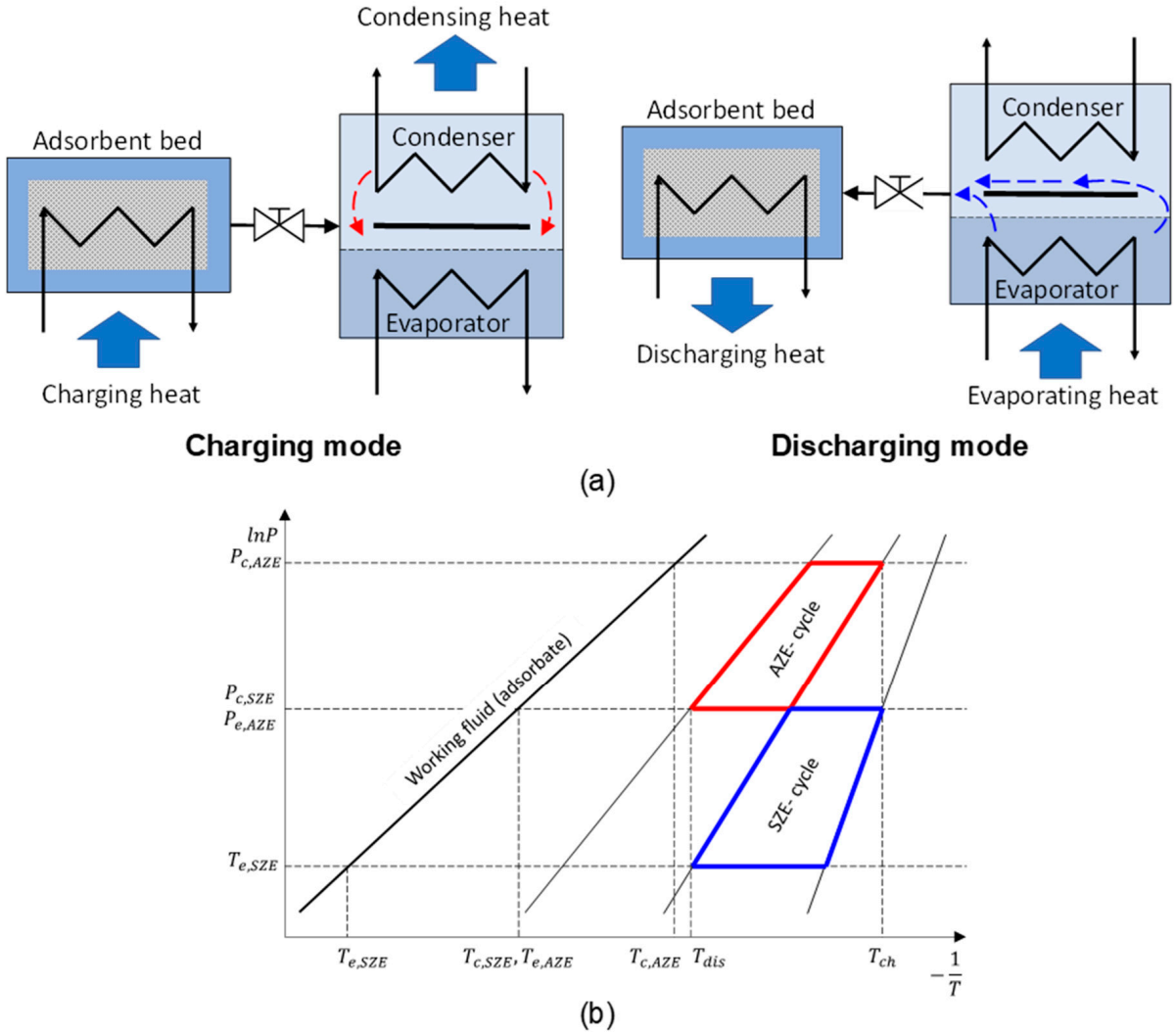

Figure 2. Clapeyron diagram for the studied heat storage cycles.

This study considered two cycles: above-zero evaporation (AZE) and sub-zero evaporation (SZE) heat storage cycle. In AZE, the ambient temperature of 10 °C was considered, which acts as a heat source for the evaporator at 5 °C and heat sink for the condenser at 15 °C. Grekova et al. [31] reported the availability of warm climates, such as southwest and southeast Asia, North Africa, and Central America. It was also reported that such a temperature is geothermally obtainable in cold climates such as Europe. The SZE cycle was investigated by utilizing ethanol as an adsorbate, given the simplicity of using the ambient as a heat source. As such, the ambient temperature of zero was considered, and the corresponding evaporation heat source and condensation heat sink temperatures are −5 °C and 5 °C, respectively. Table 1 shows the operating and equivalent ambient temperatures for AZE and SZE heat storage cycles.

Table 1. The operating and ambient temperature for the investigated heat storage cycles (AZE and SZE).

Cycle	T_{ch} [°C]	T_c [°C]	T_{dis} [°C]	T_e [°C]	T_{amb} [°C]	Adsorbate
AZE	75	15	35	5	10	Water Ethanol
SZE	75	5	35	−5	0	Ethanol

3. Results and Discussion

This section presents the experimental investigation of silica gel as a porous adsorbent paired with water and ethanol. The key characteristics are the heat of adsorption and the cyclic adsorbate uptake under predefined heat charging/discharging operating conditions. Such characteristics enable determining the heat storage potential of silica gel/ethanol to pair and benchmark it against the widely investigated silica gel/water. In addition, the exergy analysis was undertaken to understand the energy conversion quality for the investigated pairs during the entire heat charging/discharging cycle.

3.1. Heat of Adsorption

The heat of adsorption determines the exothermic/endothermic energies developed during the adsorption/desorption per mole of the up-taken/off-taken adsorbate. Therefore, by knowing the heat of adsorption, the heat storage potential can be determined using Equation (1) [31].

$$q_{storage} = \frac{\Delta W \times E_a}{M} \tag{1}$$

where ΔW denotes the cyclic water uptake (kg_{fluid}/kg_{ads}); E_a is the heat of adsorption (J/mol); M is the molar mass (kg/mol). The heat of adsorption was determined using the Clausius–Clapeyron-type equation. The surface coverage was measured by the change in adsorbent mass due to the adsorbate (i.e., water and ethanol) uptake, as shown in Figure 3. The Clausius–Clapeyron-type equation was solved by assuming merely exothermic adsorption at 10 points along the isotherms at two temperatures: T_1 = 25 °C and T_2 = 45 °C. The deferential form of the Clausius–Clapeyron-type equation at T_1 and T_2, and their corresponding pressure ratios $(P_{evap}/P_{ads})_1$ and $(P_{evap}/P_{ads})_2$ are shown in Equation (2) [32].

$$\frac{\partial ln(P/P_{bed})}{\partial T} = -\frac{E_a}{RT^2} \tag{2}$$

$$E_a = -R\frac{ln\left(\frac{(P/P_{bed})_1}{(P/P_{bed})_2}\right)}{\frac{1}{T_1} - \frac{1}{T_2}} \tag{3}$$

where R denotes the universal gas constant (J/mol·K). The average experimental heat of adsorption values for silica gel/water, and silica gel ethanol are shown in Table 2. It can be observed that the heat of adsorption for silica gel/ethanol is 5.3% less than that for silica gel/water. Moreover, the heat of adsorption for silica gel/ethanol and silica gel/water is slightly above the corresponding heat of vaporization for ethanol of 42.3 × 10^3 J/mol and water of 40.7 × 10^3 J/mol at 25 °C, which to an extent manifest the multilayer condensation phenomenon where the adsorbate molecules are not all in contact with the pore surfaces. The heat of adsorption results agrees with those obtained by Rezk et al. [32].

Table 2. The experimentally determined heat of adsorption.

Pair	Heat of Adsorption (J/mol)	Standard Deviation (J/mol)
Silica gel/water	4.43 × 10^4	5.70 × 10^3
Silica gel/ethanol	4.49 × 10^4	1.92 × 10^3

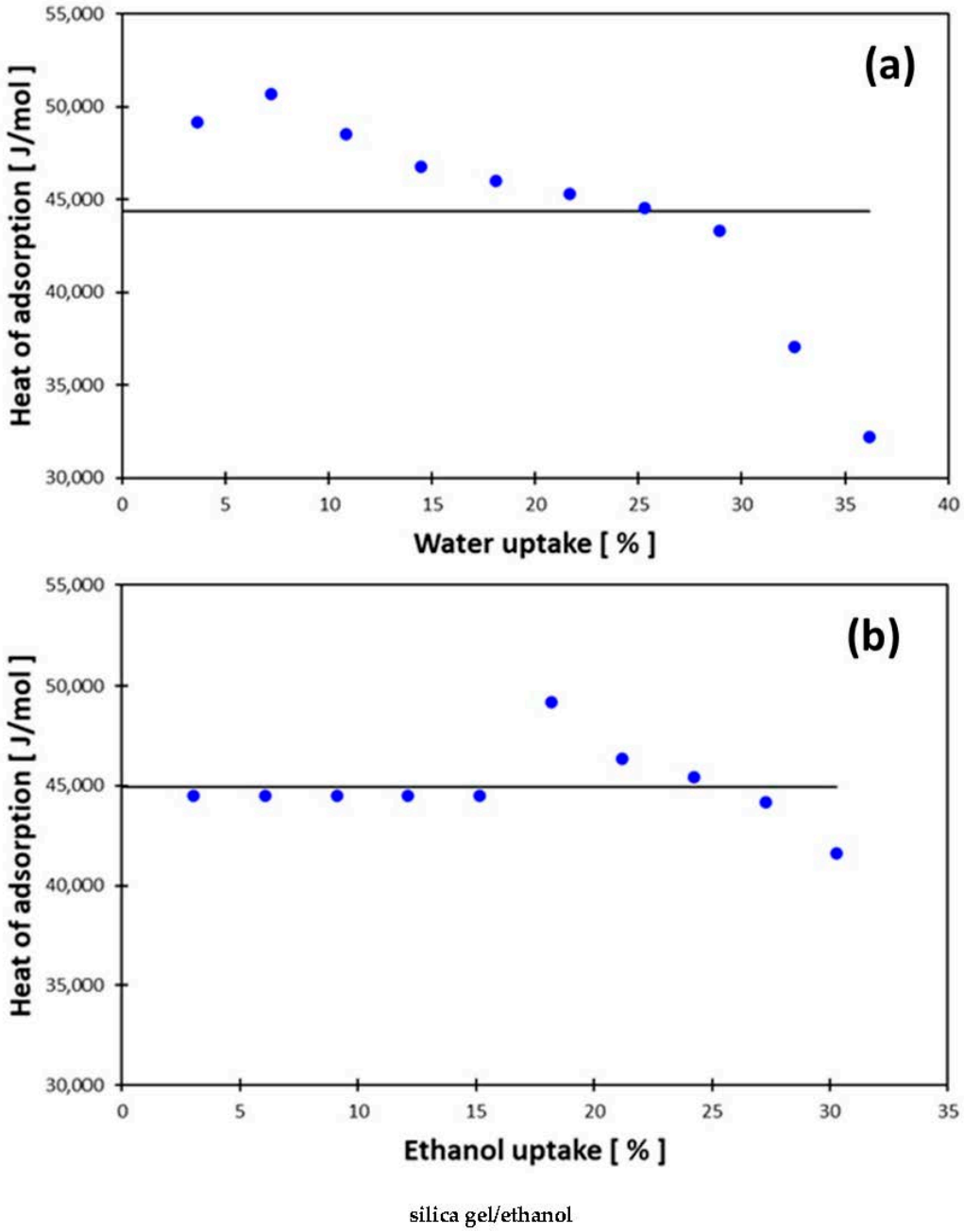

Figure 3. Plot the isosteric heat of adsorption versus the surface coverage of the (**a**) silica gel/water and (**b**) silica gel/ethanol.

3.2. Heat Storage Capacity

Figure 4 presents the heat storage cycles imposed on the equilibrium isotherm curves for silica gel/water under AZE, silica gel/ethanol under AZE, and silica gel/ethanol under SZE; this is to assess the heat storage capacity potential for each pair. It can be observed that silica gel/ethanol under SZE showed the highest net cyclic uptake potential of 0.1 $kg_{ethanol}/kg_{ads}$ followed by silica gel/water under AZE of 0.05 kg_{w}/kg_{ads} and silica gel/ethanol under AZE showed the most minor cyclic water uptake of 0.03 $kg_{ethanol}/kg_{ads}$. Considering the heat of adsorption and molecular weight for water and ethanol adsorbates yields heat storage potentials of 136.8 kJ/kg_{ads} for silica gel/water under AZE, 32.2 kJ/kg_{ads} for silica gel/ethanol under AZE and 94.6 kJ/kg_{ads} for silica gel/ethanol under SZE.

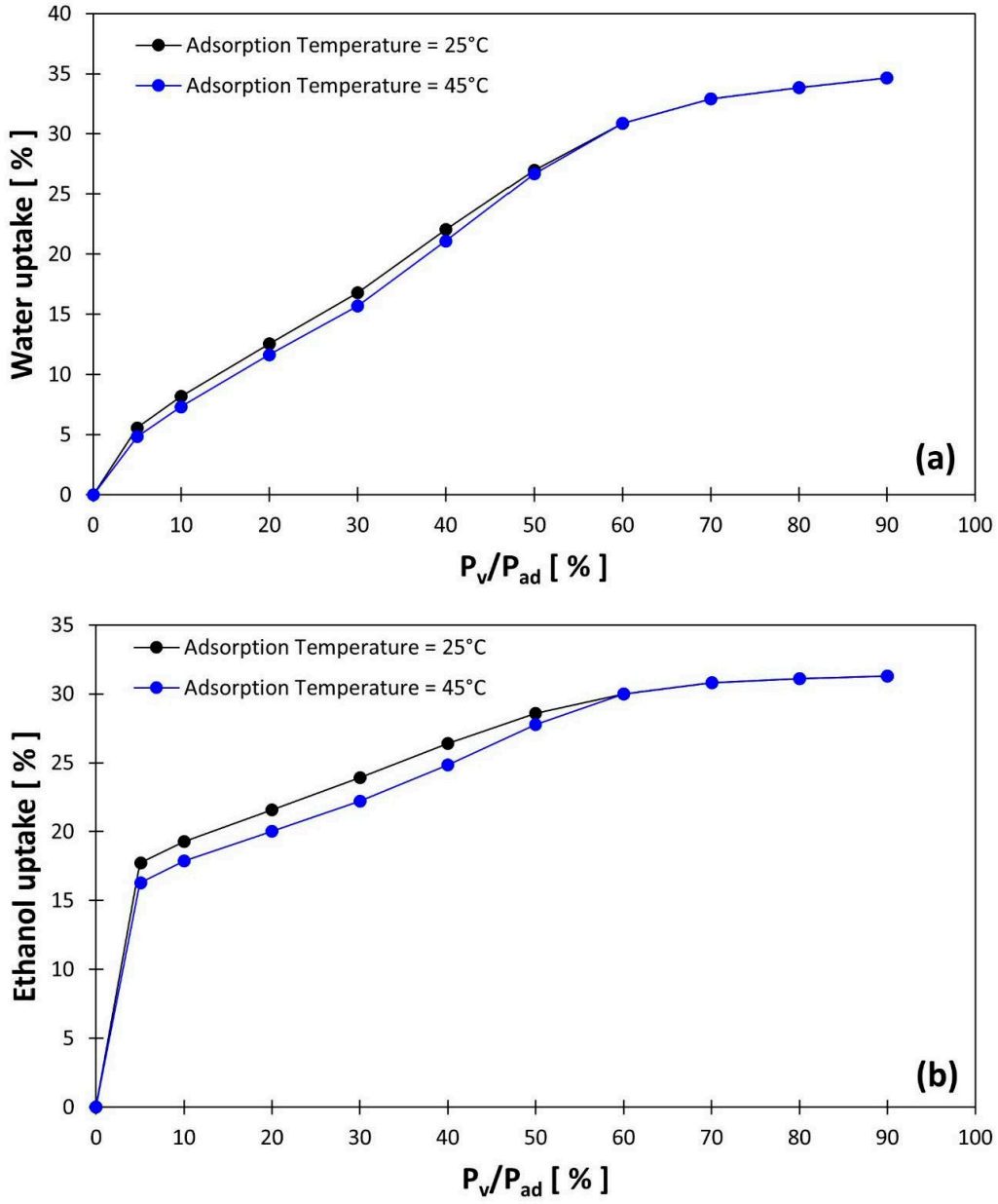

Figure 4. Adsorption isotherms for (**a**) silica gel/water and (**b**) silica gel/ethanol.

Despite determining the net cyclic water and ethanol equilibrium uptake potential enabled estimating the heat storage capacity under AZE and SZE, it did not consider the kinetics of each adsorbate during the heat charging/discharging processes. Therefore, the DVS apparatus was utilized to simulate the temporal heat charging/discharging processes by operating each pair under the realistic pressure ratios corresponding to P_{evap}/P_{ads} during the heat discharging and P_{cond}/P_{des} during heat discharging of the predefined AZE and SZE cycle conditions. The heat charging/discharging cycle time was considered 360 min to benchmark the investigated pairs. As such, Figure 5 shows the adsorbate dynamic uptake during the heat charging/discharging for silica gel/water operates under AZE cycle conditions, and silica gel/ethanol operates under AZE and SZE cycle conditions.

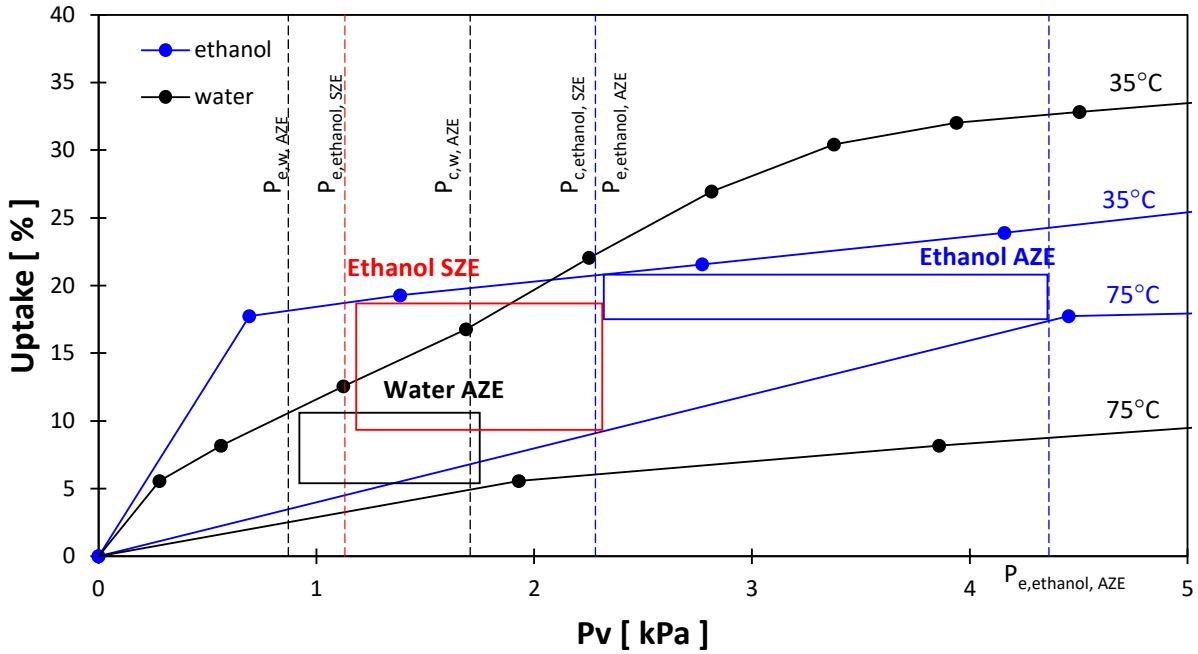

Figure 5. Equilibrium net cyclic adsorbate uptake: water AZE—black, ethanol AZE—blue, and ethanol SZE—red.

Figures 6 and 7 show the temporal cyclic adsorbate uptake and the corresponding net cyclic uptake and heat storage capacity for each pair, considering an adsorption/desorption cycle time of 360 min. Although the molecular–mass-based heat of adsorption difference between the two pairs was 5.3%, and the equilibrium cyclic uptake analysis showed that the equilibrium uptake for silica gel/ethanol under SZE outperformed silica gel water, after considering the kinetic performance under the predefined cyclic operation silica gel/ethanol showed less net cyclic water uptake of 0.025 $kg_{ethanol}/kg_{ads}$ and 0.019 $kg_{ethanol}/kg_{ads}$ in cases of AZE and SZE cycles, respectively. However, silica gel/water operated under the AZE cycle showed net cyclic uptake of 0.059 kg_w/kg_{ads}.

Ethanol is a more complex adsorbate of larger molecular size than water. It has a molar mass of 46.07 g/mol and approximately 3.6 Å molecular size, while the molar mass of water is 18.02 g/mol and its molecular size is approximately 2.75 Å. These factors adversely affected the physical mobility of ethanol molecules to reach the micropores, as reported by Rezk et al. [32], which led to a degree of non-desorbed ethanol. In this investigation, the degree of non-desorbed ethanol was more influential in the case of SZE conditions as the difference between P_v/P_{ads} and P_v/P_{des} ratios was greater in the case of AZE that reduced the net cyclic ethanol uptake and, hence, the heat storage capacity. Such physical properties resulted in a higher heat storage capacity in the case of silica gel/water of 155 kJ/kg_{ads}, while the heat storage capacity for the case of silica gel/ethanol was 24 kJ/kg_{ads} and 18 kJ/kg_{ads} under AZE and SZE cycles, respectively. Nevertheless, the benefit of using ethanol is to utilize a sub-zero ambient heat source for the evaporator.

From the desorption/adsorption kinetics, it can be observed that the rate of water offtake/uptake during heat charging/discharging for silica gel/water was slower than that for silica gel/ethanol. This is because water vapor accesses larger microporous sites that were not actively accessible by ethanol. However, from the application viewpoint silica gel/ethanol pair responded faster to the heat charging/discharging, leading to about 45% shorter cycle time potential to capture and release the heat to meet the demand. This led to a finding that silica gel with other porous structures can benefit from the high affinity of ethanol and its fast response to store larger quantities of heat.

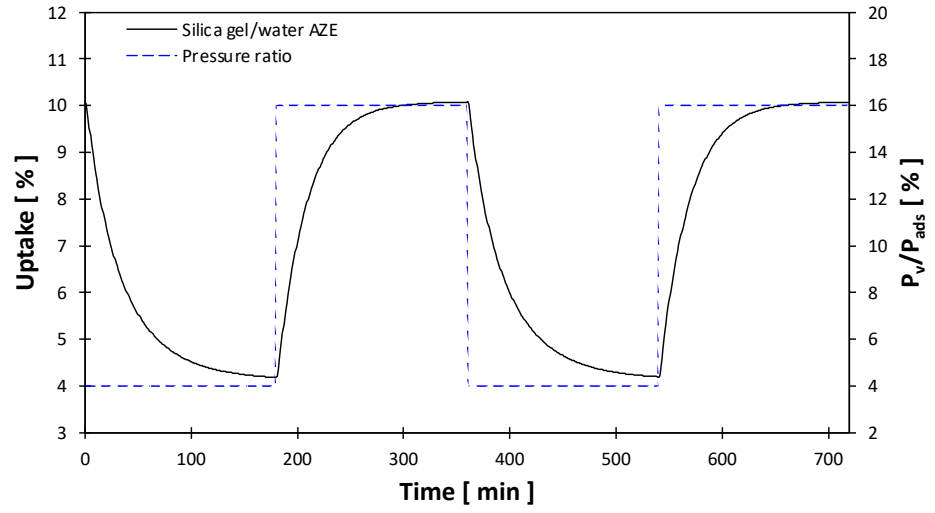

(**a**)

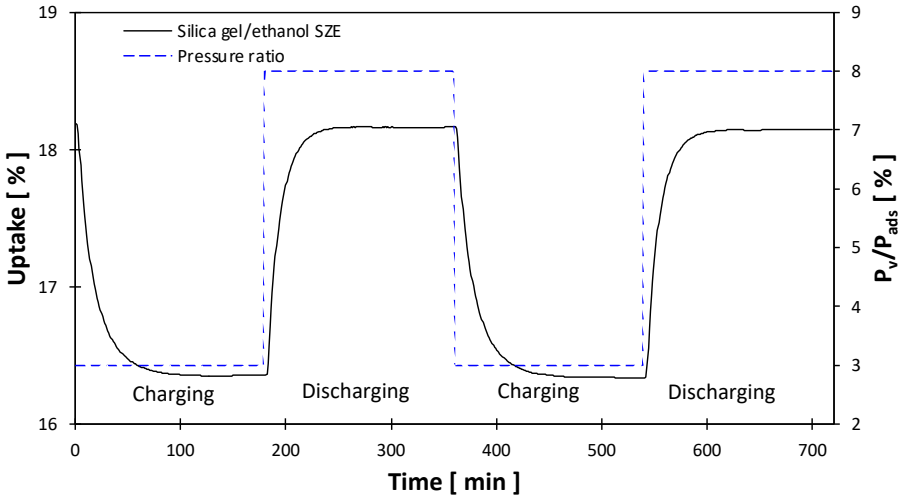

(**b**)

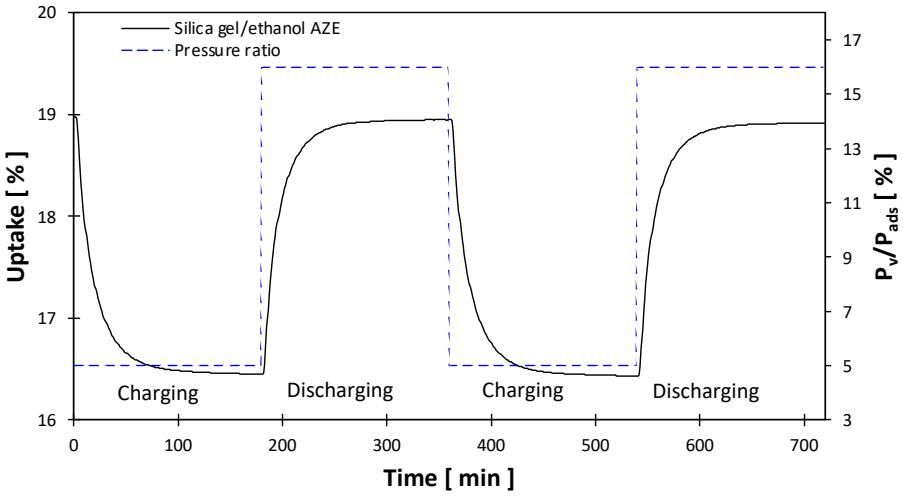

(**c**)

Figure 6. Heat chagrining/discharging cycles for (**a**) silica gel/water AZE, (**b**) silica gel/ethanol AZE and (**c**) silica gel/ethanol SZE.

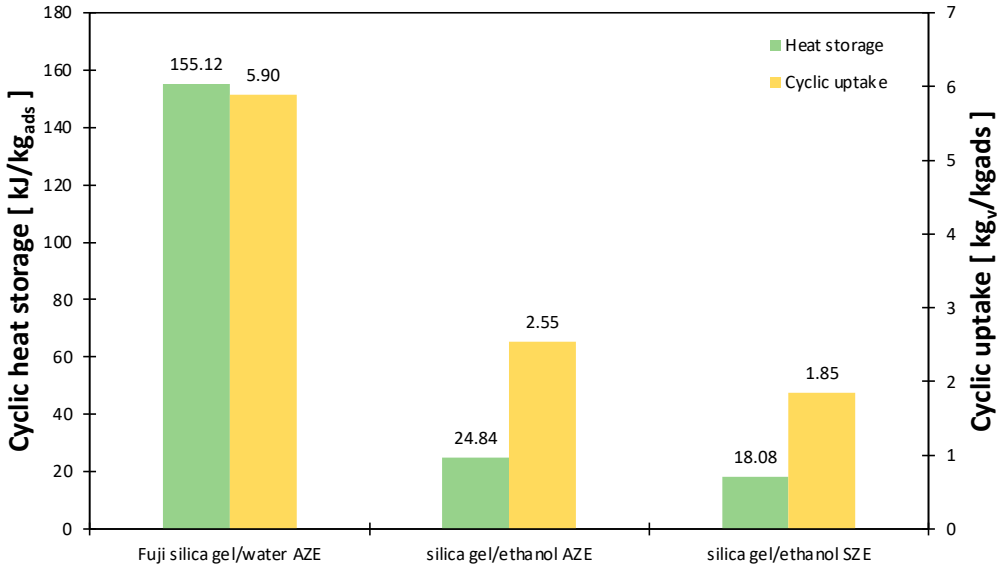

Figure 7. Heat charging/discharging cyclic performance.

3.3. Exergy Analysis

The energy conversion quality for silica gel/water and silica gel/ethanol was assessed via the exergy analysis. During the adsorption process (i.e., heat discharge), saturated water vapor at evaporator pressure is admitted into the adsorbent container, while saturated water vapor at condenser pressure leaves the container during the desorption (i.e., heat charging). As such, Equation (4) was used to undertake the exergy balance over an entire heat charging/discharging cycle [34]. Considering the ambient temperature of 300 K, the exergy destruction was constituted from the exergy transfer due to the charging/discharging heat, as shown in the first term on the right-hand side, and the exergy change of the water vapor between the inlet and exit conditions. The exergy change is constituted by the enthalpy, as shown in the second term on the right-hand side, and entropy changes between the vapor inlet and exit, as shown in the third term on the right-hand side.

$$\begin{aligned} Ex_{destruction} = & \sum_{t=0}^{t=t_{cycle}} \left[\left(1 - \frac{T_0}{T_{des}}\right) \cdot \frac{dw_{ch} E_a}{M} \right] - \left[\left(1 - \frac{T_0}{T_{ads}}\right) \cdot \frac{dw_{dis} E_a}{M} \right] \\ & - \left(dw_{ch} h_{g,c} - dw_{dis} h_{g,e}\right) \\ & + T_0 \left(dw_{ch} s_{g,c} - dw_{dis} s_{g,e}\right) \end{aligned} \quad (4)$$

where $Ex_{destruction}$ denotes the exergy destruction over the heat charging/discharging cycle; t_{cycle} is the heat charging/discharging time; T_0 is the ambient temperature; $h_{g,c}$ is the specific enthalpy of the saturated vapor leaving the adsorption reactor to the condenser; $h_{g,e}$ is the specific enthalpy of the saturated vapor entering the adsorption reactor from the evaporator; $s_{g,c}$ is the specific entropy of the saturated vapor leaving the adsorption reactor to the condenser; $s_{g,e}$ is the specific entropy of the saturated vapor entering the adsorption reactor from the evaporator.

Given that the primary focus is on heat charging/discharging, Figure 8 shows the dynamic exergy transfer during the charging and discharging process for silica gel/water under AZE conditions and silica gel/ethanol under AZE and SZE conditions. It can be observed that the exergy transfer levels during the heat charging are higher than the discharging, primarily due to the higher temperature of charging than discharging process. The exergy transfer for the silica gel/water under AZE conditions was higher than that for silica gel/ethanol under AZE and SZE conditions, averagely by 479% and 684%, respectively. The higher exergy transfer for the silica gel/water per unit mass of silica gel was due to the higher magnitudes of charging/discharging heat. Moreover, the rate of exergy transfer was steeper in the case of silica gel/ethanol due to the high affinity of silica

gel towards it but hampered due to the poor mobility of ethanol molecules in silica gel pores, as mentioned above.

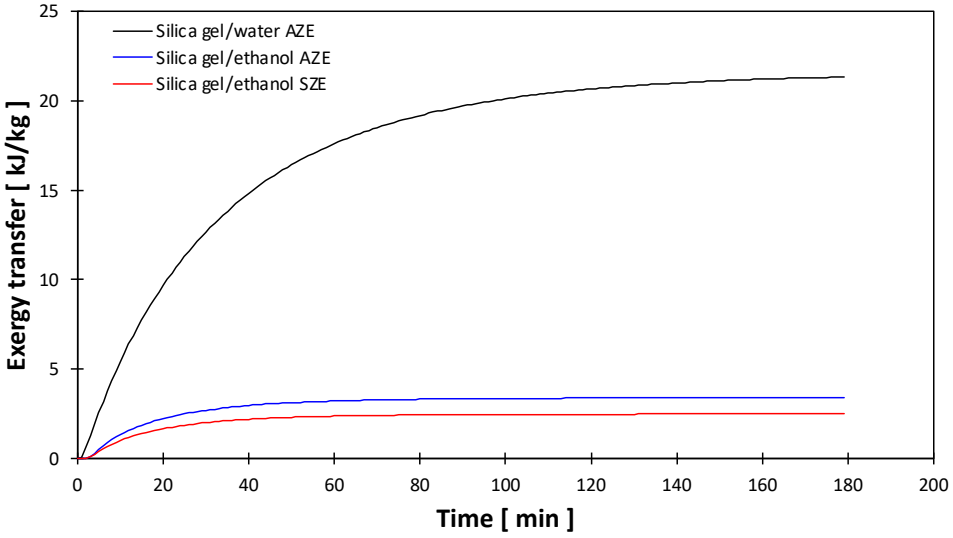

(**a**)

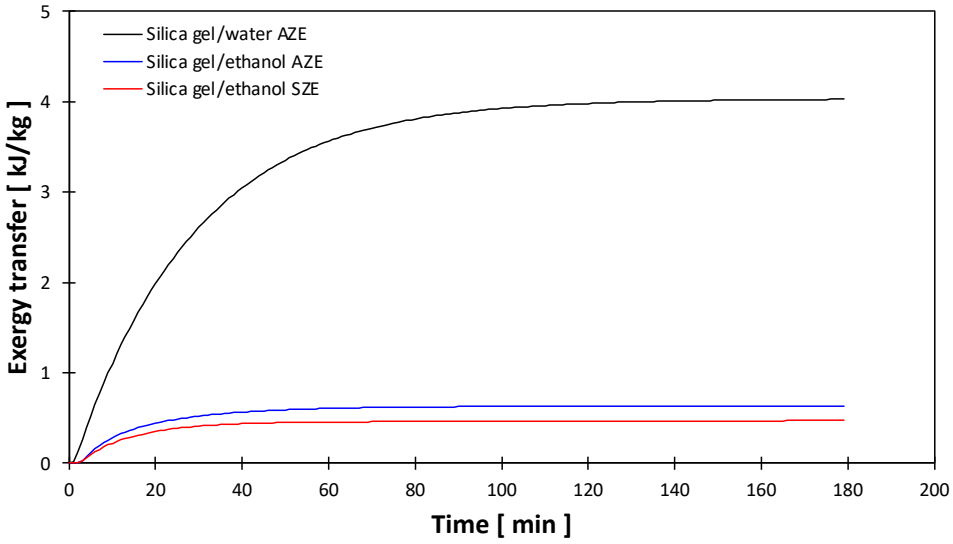

(**b**)

Figure 8. Exergy transfer during (**a**) heat charging and (**b**) heat discharging.

Figure 9 shows the magnitude of the exergy transfer and exergy change over the entire heat charging/discharging cycle and their implication in the exergy destruction. It can be observed that the main contributor to the exergy destruction was the charging heat due to the relatively high charging temperature of 75 °C. Despite the magnitude of charging and discharging heat being equal due to the reversibility of adsorption/desorption processes for silica gel/water and silica gel/ethanol, the contribution of discharging heat was the least, primarily due to the relatively low discharging heat temperature of 35 °C. The charging and discharging exergy transfer per unit mass of silica gel for silica gel/water under AZE was 527% and 540% higher than silica gel/ethanol under AZE and 752% and 757% higher than silica gel/ethanol under SZE. The exergy change for silica gel/water under AZE was 522% and 696% higher than silica gel/ethanol under AZE and SZE due to the greater cyclic water vapor uptake/offtake for the former. The effect of exergy transfer and exergy change

led to 11.87 kJ/kg_{ads} exergy destruction for silica gel/water under AZE, which was 528% and 773% higher than silica gel/ethanol under AZE and SZE, respectively.

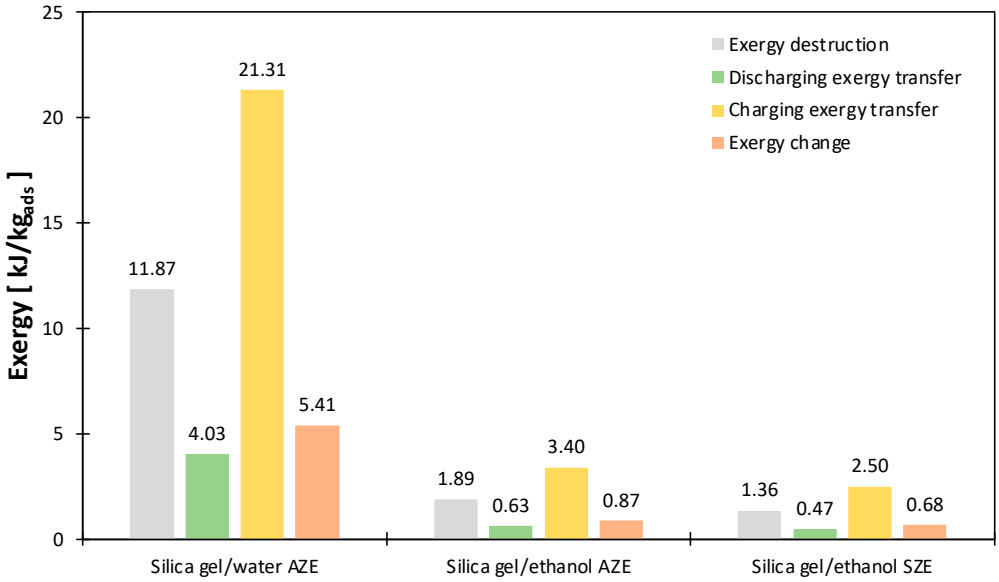

Figure 9. Breakdown of exergy destruction during heat charging/discharging cycle.

Table 3 shows the exergy change breakup for silica gel/water and silica gel/ethanol. The contribution of exergy change due to the entropy change is higher than that due to the enthalpy change by 301%, 23%, and 42% for silica gel/water under AZE, silica gel/ethanol under AZE and silica gel/ethanol under SZE. The exergy changes due to the enthalpy change for silica gel/water under AZE were greater by 177% than silica gel/ethanol under AZE and by 286% than silica gel/ethanol under SZE. These changes reflect the changes of enthalpy of 18.3 kJ/kg_{water}, 15.3 kJ/$kg_{ethanol,}$ and 15.1 kJ/$kg_{ethanol}$ for water vapor under AZE, ethanol vapor under AZE, and ethanol vapor under SZE, respectively. The exergy changes due to the entropy change for silica gel/water under AZE were bigger by 802% than silica gel/ethanol under AZE and by 983% than silica gel/ethanol under SZE. These changes reflect the changes of entropy of 0.24 kJ/kg_{water} and 0.06 kJ/$kg_{ethanol}$ under AZE. The entropy change for ethanol vapor under SZE was 0.07 kJ/$kg_{ethanol}$. Although the entropy change for ethanol under SZE was marginally greater than ethanol under AZE by 17%, the magnitude of ethanol uptake was 38% less than for ethanol vapor under AZE, which led to a relatively lower exergy change. The percentage contribution for silica gel/ethanol under SZE of 59% was, however, higher than silica gel/ethanol under AZE of 55%.

Table 3. Breakup of the exergy change and enthalpy and entropy percentage contributions over the entire heat charging/discharging cycle.

	$\sum_{ch/dis}(dw_{ch}h_{g,c} - dw_{dis}h_{g,e})$		$\sum_{ch/dis} T_0(dw_{ch}s_{g,c} - dw_{dis}s_{g,e})$	
	[kJ/kg_{ads}]	**[%]**	**[kJ/kg_{ads}]**	**[%]**
Silica gel/water AZE	1.08	20%	4.33	80%
Silica gel/ethanol AZE	0.39	45%	0.48	55%
Silica gel/ethanol SZE	0.28	41%	0.40	59%

4. Conclusions and Prospects

This study aimed to understand the heat storage potential of silica gel/ethanol to meet the heat storage demands in geographical locations of sub-zero ambient, emphasizing short-term heat storage, and benchmark it against the widely investigated silica gel/water. The heat storage characteristics, heat charging/discharging cyclic performance, and energy

conversion performance via exergy analysis of both adsorption pairs under realistic cyclic operating conditions were experimentally determined. Accordingly, the findings of this study are concluded below.

- Ethanol is a viable working fluid for adsorption heat storage to utilize the sub-zero ambient conditions without needing an underground heat source for the evaporator.
- Silica, gel/ethanol under SZE, showed the most significant net equilibrium cyclic uptake of double the equilibrium for silica gel/water and more than three times for silica gel/ethanol under AZE. On the other hand, a degree of non-desorbed ethanol during the charging process occurred, which affected the quasi-realistic cyclic uptake hence the heat storage capacity of the silica gel/ethanol pair. Such an effect stemmed from the large molecular size of ethanol for the high microporosity level of the investigated silica gel.
- Ethanol adsorbate has a high affinity towards silica gel, resulting in faster adsorption/desorption process and hence faster discharging/charging processes, which flags that utilizing silica gel of other porous structures of more accessible sites for ethanol molecules can enable faster heat charging/discharging rate along with the magnitude of heat storage capacity.
- The exergy transfer during the heat charging process was the primary contributor to the exergy destruction due to the high-temperature level and heat quantities. On the contrary, the exergy transfer during heat discharging was the minor contributor to the exergy destruction, albeit the amount of heat discharging was equal to that for charging. Therefore, it is concluded that the degree of heat (i.e., temperature) dominates the exergy transfer contribution.
- The entropy change during the charging and discharging processes was the main contributor to the breakup of exergy change.
- Given the potential of utilizing ethanol as a working fluid for adsorption heat storage, future work will revolve around pairing ethanol with porous materials of various structures aiming to fast charging/discharging responses simultaneously with heat storage quantities.

Author Contributions: Conceptualization, A.R. (Ahmed Rezk) and H.D.; methodology, A.R. (Ali Radwan), A.H.A., A.R. (Ahmed Rezk) and H.D.; formal analysis, S.M.A.R., S.K.S. and M.A.A.; investigation, A.G.O., S.M.A.R. and M.A.A.; resources, S.M.A.R., S.K.S., M.A.A. and A.H.A.; data curation, A.H.A. and A.R. (Ahmed Rezk); writing—original A.R. (Ali Radwan), A.G.O., A.H.A., A.R. (Ahmed Rezk), H.D., S.M.A.R., S.K.S. and M.A.A.; draft preparation, A.R. (Ahmed Rezk), A.G.O., A.H.A., A.R. (Ali Radwan), H.D., S.M.A.R., S.K.S. and M.A.A. All authors have read and agreed to the published version of the manuscript.

Funding: This work was supported by the University of Sharjah, project no. 19020406129.

Conflicts of Interest: The authors declare no conflict of interest.

References

1. Olabi, A.G.; Wilberforce, T.; Elsaid, K.; Sayed, E.T.; Maghrabie, H.M.; Abdelkareem, M.A. Large scale application of carbon capture to process industries—A review. *J. Clean. Prod.* **2022**, *362*, 132300. [CrossRef]
2. Rehman, A.u.; Lal, B. Gas Hydrate-Based CO_2 Capture: A Journey from Batch to Continuous. *Energies* **2022**, *15*, 8309. [CrossRef]
3. Abdelkareem, M.A.; Maghrabie, H.M.; Sayed, E.T.; Kais, E.-C.A.; Abo-Khalil, A.G.; Radi, M.A.; Baroutaji, A.; Olabi, A.G. Heat pipe-based waste heat recovery systems: Background and applications. *Therm. Sci. Eng. Prog.* **2022**, *29*, 101221. [CrossRef]
4. Elahi, M.A.E.; Mahmud, T.; Alam, M.M.; Hossain, M.J.; Biswas, B.N. Exergy Analysis of Organic Rankine Cycle for Waste Heat Recovery Using Low GWP Refrigerants. *Int. J.* **2022**, *16*, 100243. [CrossRef]
5. Dai, R.; Chen, G.; Wei, K.; Chen, Z.; Lv, X.; Liu, G.; Li, Y.; Geng, S. Effect of chemical reactions between electrolyte and lithium compounds on the electrochemical performance of the ceramic fuel cells. *Carbon Resour. Convers.* **2022**, *5*, 131–138. [CrossRef]
6. Evangelisti, L.; De Lieto Vollaro, R.; Asdrubali, F. Latest advances on solar thermal collectors: A comprehensive review. *Renew. Sustain. Energy Rev.* **2019**, *114*, 109318. [CrossRef]
7. Ravi Kumar, K.; Krishna Chaitanya, N.V.V.; Sendhil Kumar, N. Solar thermal energy technologies and its applications for process heating and power generation—A review. *J. Clean. Prod.* **2021**, *282*, 125296. [CrossRef]

8. Awasthi, A.; Shukla, A.K.; Manohar, S.R.M.; Dondariya, C.; Shukla, K.N.; Porwal, D.; Richhariya, G. Review on sun tracking technology in solar PV system. *Energy Rep.* **2020**, *6*, 392–405. [CrossRef]
9. Lund, J.W.; Toth, A.N. Direct utilization of geothermal energy 2020 worldwide review. *Geothermics* **2021**, *90*, 101915. [CrossRef]
10. Soltani, M.; Moradi Kashkooli, F.; Souri, M.; Rafiei, B.; Jabarifar, M.; Gharali, K.; Nathwani, J.S. Environmental, economic, and social impacts of geothermal energy systems. *Renew. Sustain. Energy Rev.* **2021**, *140*, 110750. [CrossRef]
11. Ahmed, S.D.; Al-Ismail, F.S.M.; Shafiullah, M.; Al-Sulaiman, F.A.; El-Amin, I.M. Grid Integration Challenges of Wind Energy: A Review. *IEEE Access* **2020**, *8*, 10857–10878. [CrossRef]
12. Jiang, L.; Lin, Y.C.; Liu, W.; Ma, Z.W.; Wang, R.Q.; Zhang, X.J.; Roskilly, A.P. Thermophysical characterization of magnesium chloride and its application in open sorption thermal energy storage system. *Sol. Energy Mater. Sol. Cells* **2022**, *236*, 111528. [CrossRef]
13. Nienborg, B.; Helling, T.; Fröhlich, D.; Horn, R.; Munz, G.; Schossig, P. Closed Adsorption Heat Storage—A Life Cycle Assessment on Material and Component Levels. *Energies* **2018**, *11*, 3421. [CrossRef]
14. Gao, N.; Deng, L.; Li, J.; Huang, H.; Zhou, B.; Zhou, Y. Multi-form heat storage performance of expanded graphite based $CaCl_2$ composites for low-grade heat source. *Energy Rep.* **2022**, *8*, 12117–12125. [CrossRef]
15. Wolf, V.; Bertrand, A.; Leyer, S. Analysis of the thermodynamic performance of transcritical CO_2 power cycle configurations for low grade waste heat recovery. *Energy Rep.* **2022**, *8*, 4196–4208. [CrossRef]
16. Yu, N.; Wang, R.Z.; Wang, L.W. Sorption thermal storage for solar energy. *Prog. Energy Combust. Sci.* **2013**, *39*, 489–514. [CrossRef]
17. Banaei, A.; Zanj, A. A Review on the Challenges of Using Zeolite 13X as Heat Storage Systems for the Residential Sector. *Eneriges* **2021**, *14*, 8062. [CrossRef]
18. Elias, C.N.; Stathopoulos, V.N. A comprehensive review of recent advances in materials aspects of phase change materials in thermal energy storage. *Energy Procedia* **2019**, *161*, 385–394. [CrossRef]
19. Zahid, M.S.; Ahmed, N.; Qaisrani, M.A.; Mahmood, M.; Ali, M.; Waqas, A.; Assadi, M. Charging and discharging characterization of a novel combined sensible-latent heat thermal energy storage system by experimental investigations for medium temperature applications. *J. Energy Storage* **2022**, *55*, 105612. [CrossRef]
20. El-Kaddadi, L.; Asbik, M.; Zari, N.; Zeghmati, B. Experimental study of the sensible heat storage in the water/TiO_2 nanofluid enclosed in an annular space. *Appl. Therm. Eng.* **2017**, *122*, 673–684. [CrossRef]
21. Olabi, A.G.; Elsaid, K.; Sayed, E.T.; Mahmoud, M.S.; Wilberforce, T.; Hassiba, R.J.; Abdelkareem, M.A. Application of nanofluids for enhanced waste heat recovery: A review. *Nano Energy* **2021**, *84*, 105871. [CrossRef]
22. Pinel, P.; Cruickshank, C.A.; Beausoleil-Morrison, I.; Wills, A. A review of available methods for seasonal storage of solar thermal energy in residential applications. *Renew. Sustain. Energy Rev.* **2011**, *15*, 3341–3359. [CrossRef]
23. Aydin, D.; Casey, S.P.; Riffat, S. The latest advancements on thermochemical heat storage systems. *Renew. Sustain. Energy Rev.* **2015**, *41*, 356–367. [CrossRef]
24. Cabeza, L.F.; Solé, A.; Barreneche, C. Review on sorption materials and technologies for heat pumps and thermal energy storage. *Renew. Energy* **2017**, *110*, 3–39. [CrossRef]
25. Abohamzeh, E.; Frey, G. Numerical Investigation of the Adsorption Process of Zeolite/Water in a Thermochemical Reactor for Seasonal Heat Storage. *Energies* **2022**, *15*, 5944. [CrossRef]
26. Schreiber, H.; Lanzerath, F.; Bardow, A. Predicting performance of adsorption thermal energy storage: From experiments to validated dynamic models. *Appl. Therm. Eng.* **2018**, *141*, 548–557. [CrossRef]
27. Zbair, M.; Bennici, S. Survey Summary on Salts Hydrates and Composites Used in Thermochemical Sorption Heat Storage: A Review. *Energies* **2021**, *14*, 3105. [CrossRef]
28. Courbon, E.; D'Ans, P.; Skrylnyk, O.; Frère, M. New prominent lithium bromide-based composites for thermal energy storage. *J. Energy Storage* **2020**, *32*, 101699. [CrossRef]
29. D'Ans, P.; Courbon, E.; Permyakova, A.; Nouar, F.; Simonnet-Jégat, C.; Bourdreux, F.; Malet, L.; Serre, C.; Frère, M.; Steunou, N. A new strontium bromide MOF composite with improved performance for solar energy storage application. *J. Energy Storage* **2019**, *25*, 100881. [CrossRef]
30. Clark, R.-J.; Farid, M. Experimental investigation into the performance of novel $SrCl_2$-based composite material for thermochemical energy storage. *J. Energy Storage* **2021**, *36*, 102390. [CrossRef]
31. Grekova, A.; Gordeeva, L.; Aristov, Y. Composite sorbents "Li/Ca halogenides inside Multi-wall Carbon Nano-tubes" for Thermal Energy Storage. *Sol. Energy Mater. Sol. Cells* **2016**, *155*, 176–183. [CrossRef]
32. Rezk, A.; Gediz Ilis, G.; Demir, H. Experimental study on silica gel/ethanol adsorption characteristics for low-grade thermal driven adsorption refrigeration systems. *Therm. Sci. Eng. Prog.* **2022**, *34*, 101429. [CrossRef]
33. Rezk, A.; Al-Dadah, R.; Mahmoud, S.; Elsayed, A. Investigation of Ethanol/metal organic frameworks for low temperature adsorption cooling applications. *Appl. Energy* **2013**, *112*, 1025–1031. [CrossRef]
34. Yunus, C.; Boles, M.; Kanoglu, M. *Thermodynamic and Engineering Approach*; MC Graw Hill Education: New York, NY, USA, 2015.

Disclaimer/Publisher's Note: The statements, opinions and data contained in all publications are solely those of the individual author(s) and contributor(s) and not of MDPI and/or the editor(s). MDPI and/or the editor(s) disclaim responsibility for any injury to people or property resulting from any ideas, methods, instructions or products referred to in the content.